JOC The Journal of Organic Chemistry

Article

pubs.acs.org/joc

Structure−Selectivity Relationship in Ruthenium-Catalyzed Regio- and Stereoselective Addition of Alkynes to Pyrazoles: An Experimental and Theoretical Investigation

Uttam Kumar Das, Subhajit Mandal, Anakuthil Anoop,* and Manish Bhattacharjee*

Department of Chemistry, Indian Institute of Technology, Kharagpur 721 302, India

Supporting Information

ABSTRACT: Ruthenium(II) complexes, $[Ru(dppe)(PPh_3)(CH_3CN)_2Cl][BPh_4]$ {dppe = diphenylphosphinoethane} (**1**) and $[Ru(dppp)_2(CH_3CN)Cl][BPh_4]$ (**2**) {dppp = diphenylphosphinopropane}, are efficient catalysts for vinylation of pyrazoles by alkynes. While the **1**-catalyzed reaction is *trans*-selective, the corresponding **2**-catalyzed reaction is *cis*-selective. The experimental results have been rationalized by density functional theory calculations.

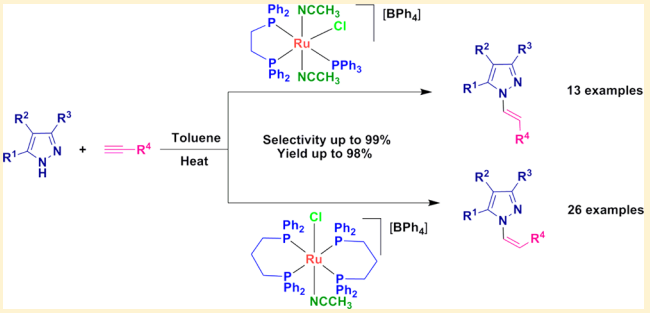

INTRODUCTION

N-Vinyl azoles have attracted great attention over the past few years because of their use in the synthesis of polymeric materials that show catalytic as well as photorefractive properties.[1] Some of the compounds also show antifungal activities.[2] It has been shown in the literature that palladium[3] and mercury[4] complexes can catalyze vinylation of azoles by vinyl bromide. However, both methods require extreme conditions. More recently, coupling of vinyl bromide/iodide and amines mediated by copper(I) in the presence of ligands and a large amount of bases such as Cs_2CO_3[5] have been developed, and the same method has been used for vinylation of azoles.[1a,d,6] Most of these methods either require harsh conditions or a long reaction time. Moreover, some of these methods require high catalyst loading. A recent report deals with copper(I)-catalyzed reactions with only 5 mol % of catalyst loading, but in most of the cases, only vinyl iodide was found to be effective.[7] Moreover, in almost all the reported methods, only (*E*)-vinyl products were obtained. It may be noted that coupling of vinyl bromide/iodide with amines is not an atom economical, environmentally friendly, and economical method because a large amount of alkali halide is produced and vinyl halides are expensive.

It was reported that $Ru_3(CO)_{10}$ can catalyze vinylation of azoles by alkynes; however, a mixture of products was obtained.[8] In a recent report, the authors found that $Ag(NO_3)/Ag(OTf)$ can catalyze single and double addition of pyrazole to alkynes. However, for single addition, the catalyst loading is high and the reaction conditions are harsh (130 °C, PhCl).[9]

Azole addition to terminal alkynes is one type of hydroamination that affords a number of possible products. Selectivity of the reaction is a central issue. Gooßen and co-workers reported that $[(cod)Ru(met)_2]$ affords (*E*)-enamides from terminal alkynes and secondary amides in the presence of a tri-*n*-butylphosphine ($P(n\text{-}Bu)_3$) ligand, but the stereoselectivity changes to the corresponding (*Z*)-enamides when a bulkier ligand such as bis(dicyclohexylphosphino)methane is used.[10]

Often, the nature of the substrate determines the regio- and stereoselectivity of a reaction. Control of regio- and stereoselectivity by the nature of the catalyst is not very common. So, catalyst-controlled product stereoselectivity is a challenge. Thus, selectivity is one of the challenging aspects in the addition reaction of terminal alkynes. We have been interested in the synthesis and catalytic activities of ruthenium phosphine complexes with hemilabile ligands, where coordinatively unsaturated species can be generated in solution.[11] Recently, in a preliminary communication, we reported the synthesis and structure of $[Ru(dppe)(PPh_3)(CH_3CN)_2Cl][BPh_4]$ {dppe = diphenylphosphinoethane} (**1**) and showed that **1** can catalyze the addition of terminal alkynes to azoles in a highly regiospecific as well stereoselective manner, and primarily (*E*)-addition products were obtained.[12] In another recent report, we described the synthesis and structure of $[Ru(dppp)_2(CH_3CN)Cl][BPh_4]$ {dppp = diphenylphosphinopropane} (**2**), which can catalyze the oxidative coupling of terminal alkynes in the presence of a catalytic amount of $Ag(NO_3)$.[13] We were interested in exploring this catalyst-structure-dependent stereospecificity of the reaction so that the (*Z*)-addition product can be obtained.

Herein, we report the structure−selectivity relationship in the vinylation of pyrazoles by alkynes catalyzed by $[Ru(dppe)(PPh_3)(CH_3CN)_2Cl][BPh_4]$ **1** and $[Ru(dppp)_2(CH_3CN)Cl][BPh_4]$ **2**. Details of the **1**-catalyzed reaction are described here. In addition, the experimental results have been rationalized by

Received: June 11, 2014
Published: October 13, 2014

dx.doi.org/10.1021/jo502151z | J. Org. Chem. 2014, 79, 9979−9991

Table 1. Catalyst Screening for the Reaction of 3,5-Dimethylpyrazole with Phenylacetylene[a]

entry	catalyst	time (h)	yield (%)[b]	E/Z[c]
1	$RuCl_3 \cdot 3H_2O + PPh_3$	24	trace	
2	$[Ru(CO)_3Cl_2]_2$	15	nr	
3	$Ru(PPh_3)_3Cl_2$	24	55	mixture
4	$Ru(PPh_3)_3Cl_2$ + dppe	24	50	1:1
5	$Ru(PPh_3)_3Cl_2$ + (1:1) dppp	12	45	2:3
6	$Ru(PPh_3)_3Cl_2$ + (1:2) dppp	12	60	1:4
7	$[Ru(PPh_3)_2(CH_3CN)_3Cl][BPh_4]$	18	62	3:2
8	$[Ru(dppe)_2(CH_3CN)Cl][BPh_4]$	12	85	1:2
9	$[Ru(dppe)(PPh_3)(CH_3CN)_2Cl][BPh_4]$	8	95	99:1
10	$[Ru(dppp)_2(CH_3CN)Cl][BPh_4]$	8	95	1:99

[a]Reaction conditions: phenylacetylene (1.5 mmol), 3,5-dimethylpyrazole (1.0 mmol), and catalyst (1 mol %) in toluene (5.0 mL) at 90 °C. [b]Isolated. [c]NMR spectroscopy.

theoretical investigations on the **1**- and **2**-catalyzed vinylation of pyrazoles by alkynes.

RESULTS AND DISCUSSION

The reaction between 3,5-dimethylpyrazole **3a** and phenyl acetylene **4a** in toluene in the presence of 1 mol % of ruthenium compound was chosen as a model reaction. A number of ruthenium compounds were tested for their efficacy as catalyst for the reaction (Table 1). While $RuCl_3 \cdot 3H_2O$ and $[Ru(CO)_4Cl_2]_2$ were found to be inactive (entries 1 and 2), $Ru(PPh_3)_3Cl_2$ and $[Ru(PPh_3)_2(CH_3CN)_3Cl][BPh_4]$ were found to be poorly active (entries 3 and 4). Somewhat better catalytic activity was observed in the cases of the combination of bidentate phosphine ligands and $Ru(PPh_3)_3Cl_2$, which afforded a low yield of 3,5-dimethyl-1-styryl pyrazole in a mixture of E/Z isomers (Table 1, entries 4–6). The complex $[Ru(dppe)_2(CH_3CN)Cl][BPh_4]$ was found to be active with better efficiency (entry 8). However, the complexes $[Ru(dppe)(PPh_3)(CH_3CN)_2Cl][BPh_4]$ (**1**) and $[Ru(dppp)_2(CH_3CN)Cl][BPh_4]$ (**2**) were found to be highly efficient. Whereas reaction in the presence of **1** produced (*E*)-3,5-dimethyl-1-styryl pyrazole (E/Z = 99:1), reaction carried out in the presence of **2** afforded (*Z*)-3,5-dimethyl-1-styryl pyrazole (E/Z = 1:99) in very high yield with high selectivity (entries 9 and 10). In the absence of ruthenium compounds, no product could be isolated. Also, the reaction carried out in the presence of Brønsted acid, triflic acid failed to give any product. These studies indicate that the reaction is catalyzed by ruthenium(II) complexes.

We next examined the optimum concentration of catalyst required for the highest conversion. We found that, in a **1**-catalyzed reaction, 0.5 mol % of catalyst loading is sufficient. However, in a **2**-catalyzed reaction, for optimum conversion, 1 mol % of catalyst loading is required. No further improvement in conversion was observed when higher catalyst loading was used. Thus, in subsequent reactions, 0.5 mol % of **1** and 1 mol % of **2** were used.

We then proceeded to examine the effect of solvent and temperature on the reaction. To begin, the reaction was carried out for 24 h at room temperature in toluene. However, we could not detect any product formation. Gradually, the temperature was increased to 70 °C, and the product could be isolated in 70% yield in 10 h. At 80 °C in 15 h, the conversion was found to be 85%. Interestingly, when the reaction temperature was increased to 90 °C, the conversion was found to be 95% in 8 h. With further increase in reaction temperature, the conversion did not improve.

The reaction in dichloromethane (DCM) or acetonitrile failed to give any product. Reaction at 80 °C in DMF and dichloroethane (DCE) led to the formation of (*Z*)-3,5-dimethyl-1-styryl pyrazole, with the conversions being 15 and 45%, respectively (Table 2).

Table 2. Solvent and Temperature Effect on Reactions of 3,5-Dimethylpyrazole with Phenylacetylene Catalyzed by 2[a]

entry	solvent	temp (°C)	time (h)	conversion (%)[b]
1	toluene	rt	24	
2	DCM	45	24	
3	acetonitrile	80	15	
4	DMF	80	15	15 (other pdt)
5	DCE	80	24	45
6	toluene	80	10	70
7	toluene	80	15	85
8	toluene	90	8	95
9	toluene	110	8	95

[a]Reaction conditions: phenylacetylene (1.5 mmol), 3,5-dimethylpyrazole (1.0 mmol), and **2** (1 mol %) in solvent (5.0 mL). [b]Isolated.

After optimizing the reaction conditions, we examined the reaction of various pyrazoles with different terminal alkynes in toluene in the presence of 0.5 mol % of **1** at 90 °C and 1 mol % of **2** at 100 °C. For convenience, the pyrazole/alkyne ratio was kept at 1:1.5, and the corresponding vinyl products were isolated in moderate to good yields. The products were characterized by ^1H and ^{13}C NMR spectroscopy and mass spectrometry. The results are given in Tables 3 and Table 4, respectively.

The reaction of pyrazole and its derivatives with terminal alkynes bearing both aliphatic and aromatic substituents, catalyzed by **1** (Table 3 and Scheme 1), afforded exclusively (*E*)-*N*-vinyl pyrazoles in most of the cases. However, the reaction of pyrazole (**3a**) with phenylacetylene (**4a**) afforded 1-styryl pyrazole (**5a**) as mixture of product (E/Z ratio = 19:1). In the reactions of 3,5-dimethylpyrazole (**3c**), 3,4,5-trimethylpyrazole (**3d**), and 3-methyl-5-phenylpyrazole (**3e**) with 1-hexyne (**4e**), a mixture of (*E*)- and (*Z*)-products was obtained (Table 3, **5d**, **5i**, **5j**), with the (*E*)-product being the major product. Similarly, the reaction of 2-but-3-ynylisoindole-1,3-dione (**4i**) with 3,5-diphenylpyrazole (**3c**) afforded a mixture of (*E*)- and (*Z*)-2-[4-(3,5-diphenylpyrazol-1-yl)but-3-enyl]isoindole-1,3-dione (**5m**). The major product was the (*E*)-product.

The reaction is highly regiospecific, as shown by the reactions of 3-methyl-5-phenylpyrazole (**3e**) with 1-hexyne (**4e**) and 2-but-3-ynylisoindole-1,3-dione (**4i**), which afford 1-hex-1-enyl-3-methyl-5-phenylpyrazole (**5j**) and 2-[4-(3-methyl-5-phenylpyrazol-1-yl)-but-3-enyl)isoindole-1,3-dione (**5k**), respectively. The substitution

dx.doi.org/10.1021/jo502151z | J. Org. Chem. 2014, 79, 9979–9991

Table 3. Vinylation of Pyrazoles Catalyzed by 1[a]

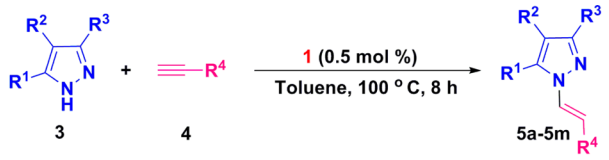

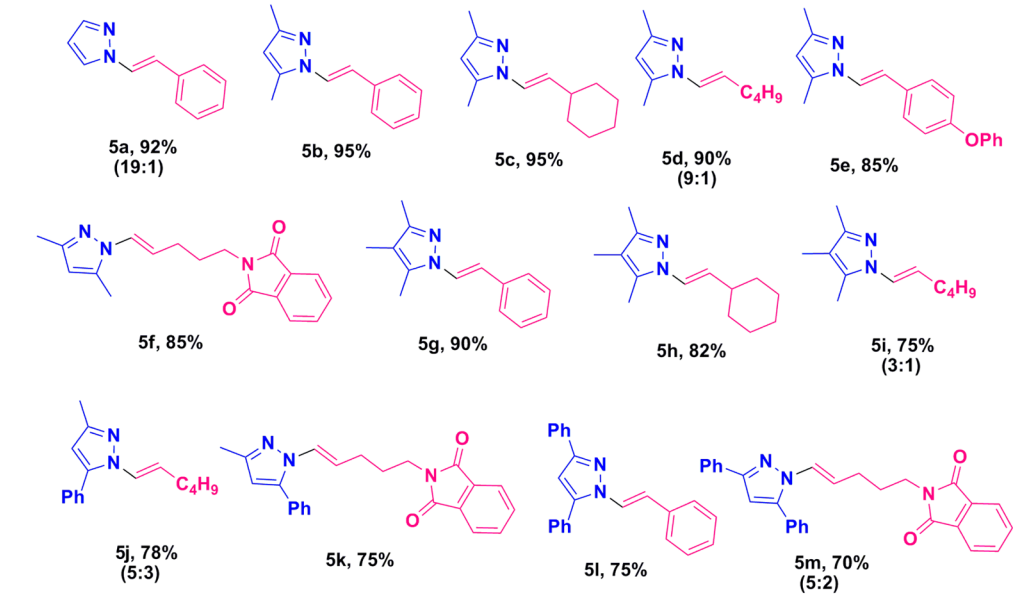

[a]Reaction conditions: alkyne (1.5 mmol), azole (1.0 mmol), **1** (0.5 mol %), and toluene (5.0 mL), T = 100 °C. Yield: Isolated. E/Z: From NMR spectroscopy.

takes place specifically at the nitrogen adjacent to the phenyl group. The regiospecificity of the substitution products was confirmed by NOESY measurements (Supporting Information). The NOESY of **5j** and **5k** shows the interaction between the vinyl proton and the phenyl proton. No interaction was observed between the vinyl proton and the methyl proton.

It may be noted that one of the products, namely, (*E*)-2-[5-(3,5-dimethylpyrazol-1-yl)pent-4-en-1-yl]isoindole-1,3-dione (**5f**), has been characterized by single-crystal X-ray crystallography.[12] The X-ray structure confirms the (*E*)-geometry of the compound.

In contrast, when **2** was used as catalyst instead of **1**, the stereoselectivity was found be opposite to that observed in the reaction catalyzed by **1** (Scheme 1). The major product was found to be the (*Z*)-isomer (Table 4). In most cases, the reaction afforded exclusively the (*Z*)-isomer, except in the case of the reaction of pyrazole (**3a**) and 3,5-dimethylpyrazole (**3c**) with 1-hexyne (**4e**) and with 1-octyne (**4f**), which afforded 1-hex-1-enylpyrazole (*E*/*Z* ratio = 1:2) (Table 4, **6d**) and 1-oct-1-enylpyrazole (*E*/*Z* ratio = 1:4) (Table 4, **6e**), and 3,5-dimthyl-1-hex-1-enylpyrazole (**6n**) (*E*/*Z* ratio = 1:2) and 3,5-dimethyl-1-oct-1-enylpyrazole (**6o**) (*E*/*Z* ratio = 2:3), respectively (Table 4). Similarly, reaction of 3,5-diphenylpyrazole (**3e**) with 1-hexyne (**4e**) afforded a 1:3 mixture (*E*/*Z*) of 3,5-diphenyl-1-hex-1-enylpyrazole (**6u**). Thus, the results show that there is an effect of the functional group, attached to the alkyne, on the stereoselectivity of the reactions.

The **2**-catalyzed reaction is also regiospecific as evidenced by the reaction of 3-methyl-1*H*-pyrazole (**3b**) and 3-methyl-5-phenyl-1*H*-pyrazole (**3f**) with phenylacetylene (**4a**), prop-2-ynyloxy benzene (**4g**), and 2-prop-2-ynylisoindole-1,3-dione (**4i**). The corresponding regiospecific products were 3-methyl-1-styryl-1*H*-pyrazole (**6i**), 3-methyl-5-phenyl-1-styryl-1*H*-pyrazole (**6s**), 3-methyl-1-(3-phenoxypropenyl)-5-phenyl-1*H*-pyrazole (**6t**), and 2-[3-(3-methyl-5-phenyl-1*H*-pyrazol-1-yl)allyl)isoindoline-1,3-dione (**6z**), respectively. The regiospecificity of the substitution reaction was confirmed from NOESY spectra of **6i**, **6s**, and **6t** (Supporting Information), where we could not observe any interaction between the methyl proton and the vinyl proton. However, we could observe the interaction between the phenyl proton and the vinyl proton in the NOESY spectra of **6s** and **6t**. Further, one of the products, (*Z*)-2-[3-(3-methyl-5-phenyl-1*H*-pyrazol-1-yl)allyl)isoindoline-1,3-dione (**6z**), has been structurally characterized.[14] The ORTEP view of the product is shown in Figure 1. The single-crystal X-ray structure confirms the stereoselectivity and regiospecificity of the reaction.

Having established the stereoselectivity and regioselectivity of **1**- and **2**-catalyzed substitution reactions, we performed density functional theory (DFT) computations to gain some insight into the possible mechanism of stereo- and regioselective vinylation of pyrazoles catalyzed by the two cationic ruthenium complexes, **1** and **2**. We have optimized all the intermediates and transition states and computed the relative energies between the competing paths. A stable minimum was found for every postulated intermediate within the catalytic cycle (Figures 2 and 4). The overall reaction mechanism is similar, although there are minor variations between the reactions catalyzed by **1** and **2**.

The catalytic cycle of **1** starts with the octahedral ruthenium(II) complex (**1_a**), where two acetonitrile ligands occupy the axial positions [Ru−N bond distances are 1.971 (AN1) and

dx.doi.org/10.1021/jo502151z | J. Org. Chem. 2014, 79, 9979−9991

Table 4. Vinylation of Pyrazoles Catalyzed by 2[a]

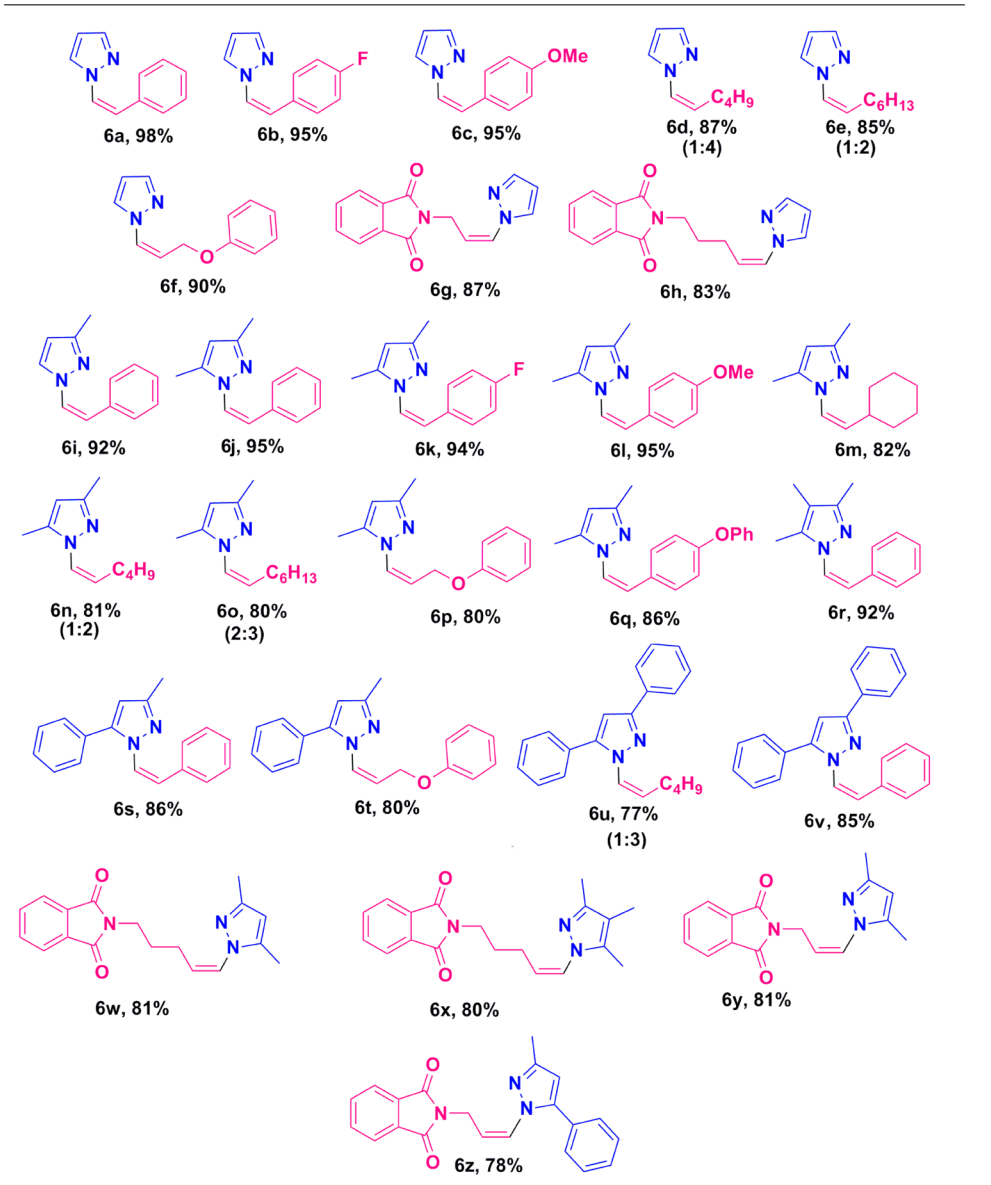

[a]Reaction conditions: alkyne (1.5 mmol), pyrazole (1.0 mmol), **2** (1 mol %), and toluene (5.0 mL), T = 90 °C. Yield: Isolated. E/Z: From NMR spectroscopy.

Scheme 1. Stereo- and Regioselective Vinylation of Pyrazoles Catalyzed by 1 and 2

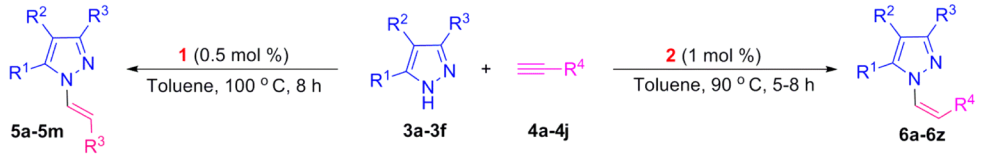

3a: $R^1 = R^2 = R^3 = H$; **3b**: $R^1 = R^2 = H$, $R^3 = CH_3$; **3c**: $R^1 = R^3 = CH_3$, $R^2 = H$; **3d**: $R^1 = R^2 = R^3 = CH_3$; **3e**: R^1 = Ph, $R^2 = H$, $R^3 = CH_3$; **3f**: R^1 = Ph, $R^2 = H$, R^3 = Ph.

4a: R^4 = Ph; **4b**: R^4 = *p*-FC_6H_5; **4c**: R^4 = *p*-$OMeC_6H_5$; **4d**: R^4 = -*cyclo*-C_6H_{11}; **4e**: R^4 = -C_4H_9; **4f**: R^4 = -C_6H_{13}; **4g**: R^4 = -$CH_2(O)C_6H_5$; **4h**: R^4 = *p*-$OPhC_6H_5$; **4i**: R^4 = isoindole-1,3-dione-2-propyl; **4j**: R^4 = N(CH_2)-isoindole -1,3-dione.

1.964 Å (AN2)] and the equatorial positions are occupied by two phosphorus atoms of the bidentate diphenylphosphinoethane (dppe) ligand (Ru−P bond distances are 2.313 and 2.356 Å) and one phosphorus atom of triphenylphosphine (Ru−P bond distance is 2.389 Å) and a chloride (Ru−Cl bond distance is 2.469 Å).

In the initial step of the reaction, the loss of one acetonitrile group (AN1) from the axial position of the octahedral complex generates a square pyramidal structure (**1_b**), with the other having the remaining acetonitrile (AN2) group in the axial position. However, the coordinatively unsaturated species having

dx.doi.org/10.1021/jo502151z | J. Org. Chem. 2014, 79, 9979−9991

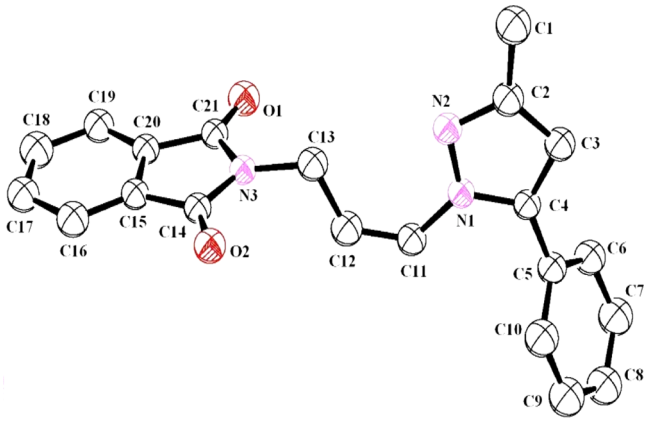

Figure 1. ORTEP view of (*Z*)-2-[3-(3-methyl-5-phenyl-1*H*-pyrazol-1-yl)allyl)isoindoline-1,3-dione (**6z**). Hydrogen atoms have been omitted for clarity.

square pyramidal geometry can be obtained either by loss of the other axial acetonitrile group (AN2) from the axial position or by loss of the equatorial PPh_3 group. However, acetonitrile is known to be more labile than the phosphine ligands.[15] Furthermore, AN1 is more loosely bound to the metal, as is evident from the longer Ru−N bond distance of AN1 compared to that of AN2 in **1_a**. The square pyramidal structure generated from the loss of AN1 is more stable than those generated from the loss of AN2 or the loss of PPh_3. The two intermediates generated from the loss of AN2 and PPh_3 are of higher energy by 2.22 and 3.05 kcal/mol, respectively, than that generated by the loss of AN1.

Our attempts to locate the transition states for the square pyramidal intermediates generated by the loss of AN1, AN2, and PPh_3 failed as the energy of the fragments increases monotonously in the relaxed surface scan. This prompted us to consider an alternative pathway: associative removal of AN1 with simultaneous addition of phenylacetylene. According to this pathway, we have studied three possibilities, loss of AN1, AN2, and PPh_3 with assistance by phenylacetylene addition. Here, AN1 loss has an activation barrier of 17.19 kcal/mol. The AN2 and PPh_3 loss has free energy barriers of 19.68 and 23.37 kcal/mol. Therefore, the AN1 removal pathway is the most feasible among these three possibilities. The geometries related to catalyst **1** are presented in Figure 3.

Ruthenium is known to form strong π-complexes with alkynes.[16−18] Uchimaru proposed a mechanism for the ruthenium-catalyzed hydroamination of terminal alkynes,[19] in which a π-coordinated alkyne inserts into the Ru−N bond of a ruthenium amine species. In another study, Caulton and co-workers[20] investigated the pathways toward the formation of a ruthenium vinylidene intermediate and have shown that π-coordinated alkynes readily insert into Ru−H bonds and form ruthenium vinyl complexes. On further rearrangement, the ruthenium vinyl species produces a ruthenium vinylidene complex. They have also proposed that for bulkier ruthenium complexes, instead of a π-complex, the vinylidine can be produced through a 1,2-hydrogen migration directly from the σ-complex.

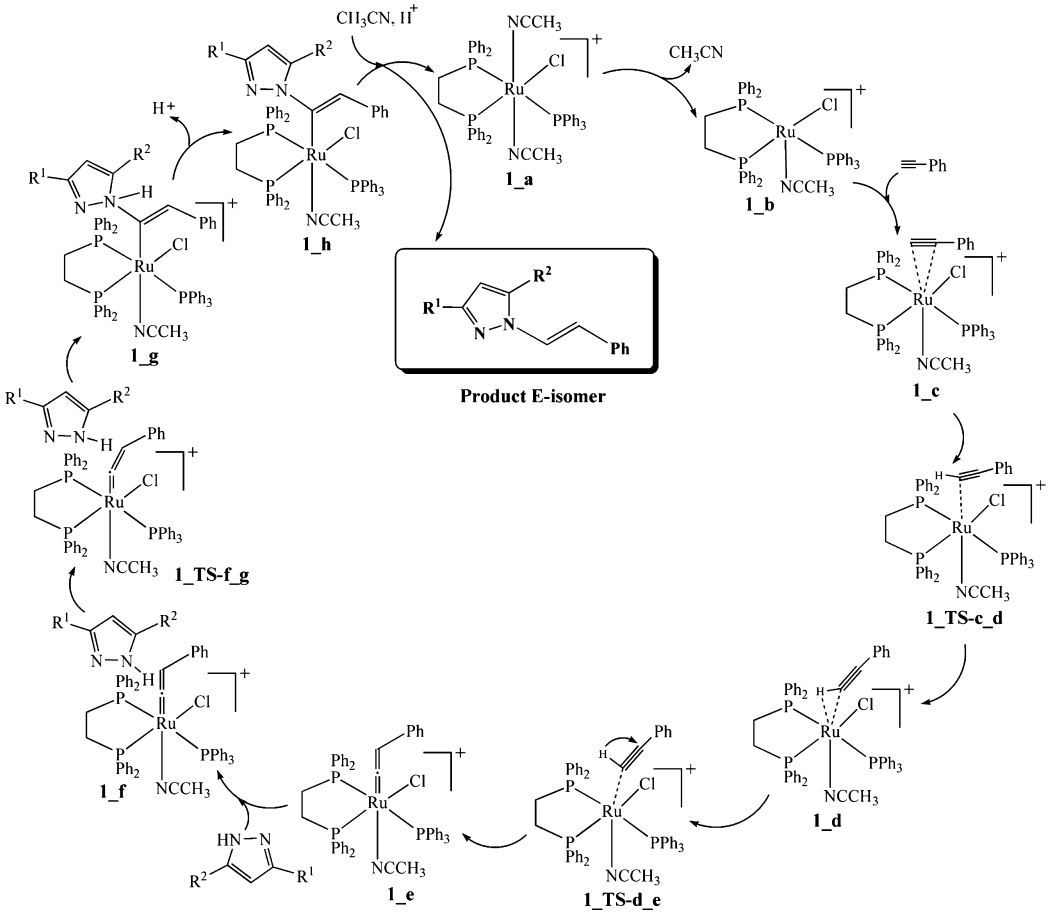

Figure 2. Mechanism for the vinylation of pyrazole in the presence of **1**.

dx.doi.org/10.1021/jo502151z | *J. Org. Chem.* 2014, 79, 9979−9991

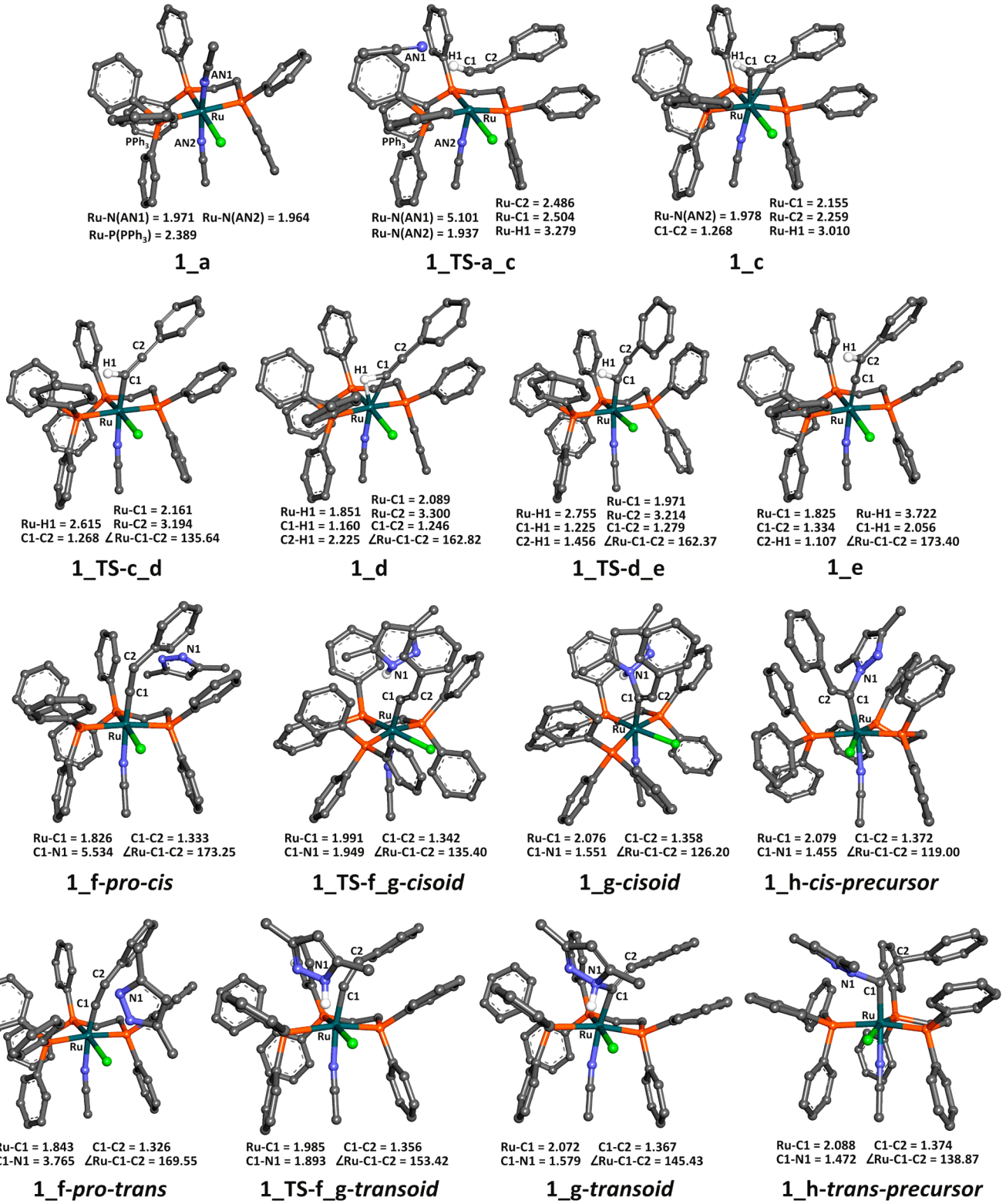

Figure 3. Geometries of the intermediates and transition states for the vinylation of pyrazole in the presence of **1**. Hydrogen atoms are not shown for clarity. Selected distances and angles are presented in angstroms and degrees, respectively.

The addition of phenylacetylene can result in either a π-complex (**1_c**) or a σ-complex (**1_d**). Relaxed surface scans between the ruthenium center and the terminal carbon of phenylacetylene suggest the formation of a π-complex, which is also thermodynamically more stable. This step is endothermic and endergonic ($\Delta_r E_{tot}$ = 6.16 kcal/mol, $\Delta_r G_{298}$ = 11.01 kcal/mol). In the π-complex, ruthenium is coordinated to phenylacetylene in an η^2 manner. The Ru−C1 and Ru−C2 bond distances in **1_c** are 2.155 and 2.259 Å, respectively (Figure 2). In the subsequent step, the π-complex rearranges to the σ-complex. Morokuma et al. studied the insertion of acetylene with ruthenium(II) and showed that acetylene first forms a π-complex, which converts to

dx.doi.org/10.1021/jo502151z | J. Org. Chem. 2014, 79, 9979−9991

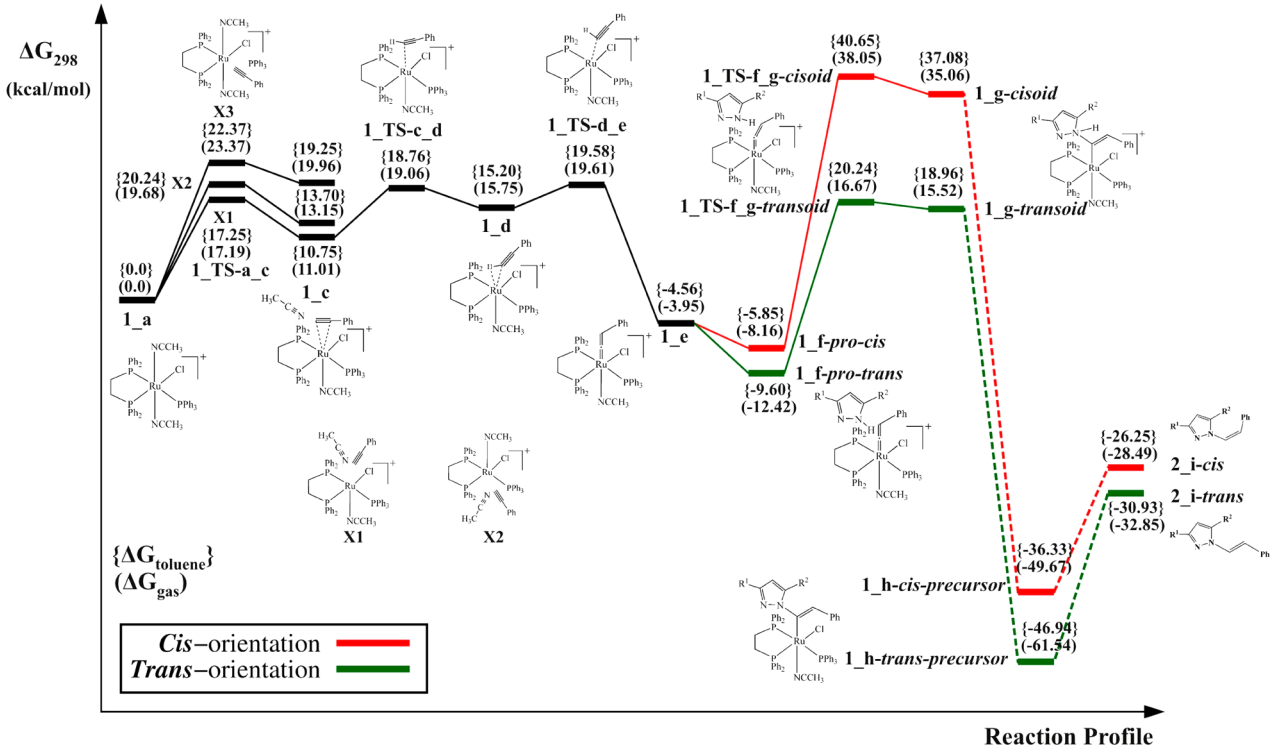

Figure 4. Free energy profile for the vinylation of pyrazole in the presence of **1**. The values presented in parentheses are ΔG_{298} in the gas phase, and the values in braces are ΔG_{298} in toluene.

σ-complex and finally 1,2-hydrogen migration produces the metal–vinylidine complex.[21] The slippage of the π-complex to the σ-complex has an activation energy barrier of $\Delta^{\ddagger}G_{298}$ = 8.05 kcal/mol. In **1_TS-c_d** geometry, the Ru–C2 bond distance increases to 3.194 Å and Ru–H1 distance decreases markedly to 2.615 Å, whereas the Ru–C1 bond distance remains almost unchanged compared to that of **1_c**. The Ru–C1 and Ru–H1 bond distances further shorten to 2.089 and 1.851 Å in **1_d**, indicating η^2 coordination of phenylacetylene.

In **1_d**, phenylacetylene is coordinated to the ruthenium center through the σ-electrons of the C1–H1 bond. The reaction energy for this step is 5.74 kcal/mol. From the σ-complex, a 1,2-hydrogen migration takes place from C1 to C2 to form the vinylidine complex (**1_e**). The hydrogen migration step has a small barrier of $\Delta^{\ddagger}G_{298}$ = 3.86 kcal/mol. In **1_TS-d_e**, the Ru–C1 bond distance further shortens to 1.971 Å, C2–H1 distance shortens to 1.456 Å, whereas the Ru–H1 distance increases to 2.755 Å. Decrease in the Ru–C1 distance indicates the formation of a ruthenium–vinylidine complex (**1_e**). In **1_e**, the Ru–C1 distance further decreases to 1.825 Å. Moreover, in **1_e**, the C1–C2 bond distance becomes 1.334 Å, which was 1.268 Å in **1_c** and 1.246 Å in **1_d**. The ruthenium–vinylidine complex (**1_e**) is a thermodynamically stable intermediate, and therefore, this step provides additional thermodynamic stability of $\Delta_r E_{tot}$ = −19.77 kcal/mol and $\Delta_r G_{298}$ = −19.70 kcal/mol.

There are two possible orientations of the added pyrazole, *pro-cis* (**1_f-*pro-cis***) or *pro-trans* (**1_f-*pro-trans***) orientation. The species **1_f-*pro-trans*** is more stable than **1_f-*pro-cis*** by 4.26 kcal/mol (Figure 4). In the following step, anti-Markovnikov addition of pyrazole nitrogen occurs on the vinylidene carbon atom α to the ruthenium(II) center. For *pro-cis* orientation, this addition step has a large barrier of $\Delta^{\ddagger}G_{298}$ = 46.21 kcal/mol. In this transition state structure (**1_TS-f_g-*cisoid***), the C1–N1 distance is 1.949 Å. However, for the *pro-trans* orientation, the activation barrier is relatively smaller, $\Delta^{\ddagger}G_{298}$ = 29.09 kcal/mol (**1_TS-f_g-*transoid***). The C1–N1 bond distance is 1.893 Å in **1_TS-f_g-*transoid***, which is significantly shorter than that in **1_TS-f_g-*cisoid*** (1.949 Å). The enormous difference between two activation barriers suggests that the pyrazole addition step is feasible only in *pro-trans* orientation. The pyrazole addition step has the highest activation barrier in the whole reaction profile. Moreover, this step regulates the stereoselectivity of the products. Therefore, the stereoselectivity-determining step is the slowest and rate-determining step.

Pyrazole addition to the ruthenium vinylidene complex generates cationic pyrazole moieties (**1_g-*cisoid*** and **1_g-*transoid***), which have energies close to the corresponding transition state energies. Removal of one proton each from **1_g-*cisoid*** and **1_g-*transoid*** geometry generates the corresponding *cis*-precursor (**1_h-*cis-precursor***) and *trans*-precursor (**1_h-*trans-precusor***) structures. This step is highly exergonic and exothermic for both the *cis*-precursor ($\Delta_r E_{tot}$ = −78.43 kcal/mol, $\Delta_r G_{298}$ = −84.73 kcal/mol) and the *trans*-precursor ($\Delta_r E_{tot}$ = −68.54 kcal/mol, $\Delta_r G_{298}$ = −77.06 kcal/mol) orientations. Additionally, the **1_h-*trans-precursor*** is more stable than the **1_h-*cis-precursor*** by $\Delta_r E_{tot}$ = −13.35 kcal/mol and $\Delta_r G_{298}$ = −11.87 kcal/mol. Finally, protonolysis of **1_h-*cis-precursor*** and **1_h-*trans-precusor*** produces the related *cis*- and *trans*-product, respectively. The free energy profile of the reaction is shown in Figure 4.

The catalytic cycle of $[Ru(dppp)_2(CH_3CN)Cl][BPh_4]$ (**2**) (Figure 5) catalyzed reaction starts with octahedral ruthenium(II) complex (**2_a**) and $[BPh_4]^-$ as the counteranion. In the octahedral complex **2_a**, acetonitrile and chloride groups occupy axial positions and two bidentate diphenylphosphinopropane (dppp) ligands occupy equatorial positions, as observed from the crystal structure.[13] In the initial step of the reaction, removal of

dx.doi.org/10.1021/jo502151z | J. Org. Chem. 2014, 79, 9979–9991

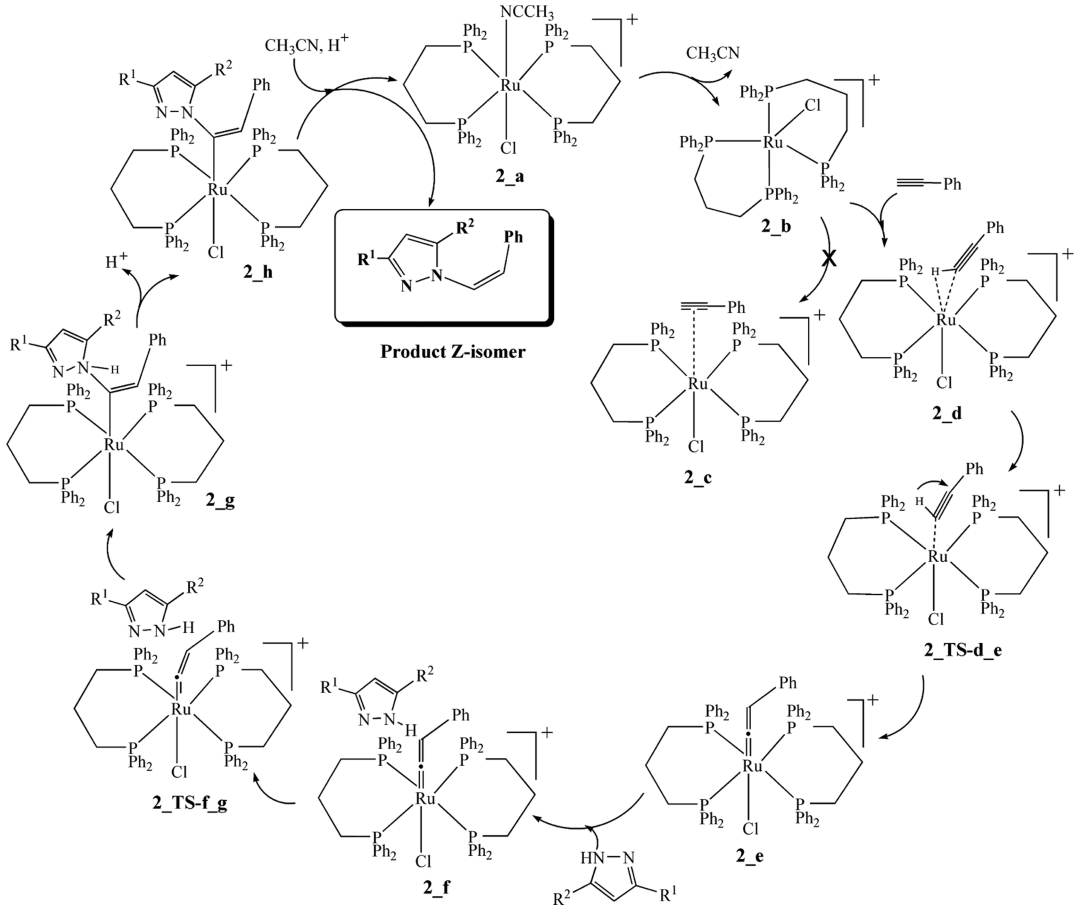

Figure 5. Mechanism of the vinylation of pyrazole in the presence of **2**.

the acetonitrile group produces a distorted trigonal bipyramidal (TBP) geometry (**2_b**), as seen in the crystal structure.[13] Because the geometry and the existence of this intermediate is proved by the crystal structure, we did not attempt to find the transition state for the removal of acetonitrile.

In the TBP structure, one phosphorus from each bidentate ligand occupies the axial positions, and the other two phosphorus and chlorine occupy the equatorial positions. The axial Ru−P bond distances (2.395 and 2.390 Å) [experimentally observed bond distances are 2.429 and 2.416 Å] are larger than the equatorial Ru−P bond distances (2.224 and 2.261 Å) [experimentally observed bond distances are 2.263 and 2.280 Å]. Removal of acetonitrile is endothermic ($\Delta_r G_{298}$ = 3.71 kcal/mol; $\Delta_r E_{tot}$ = 12.44 kcal/mol), due to the generation of a coordinatively unsaturated species. The endothermicity justifies the high-temperature reaction conditions to gain the required reaction energy.

Addition of an alkyne to the TBP intermediate (**2_b**) can result either in a π-complex (**2_c**) or a σ-complex (**2_d**) formation. Our result shows that for **2** the σ-complex is thermodynamically more favored than the π-complex by 7.37 kcal/mol. This is in contrast to the **1_c/d**, where the π-complex is more stable. In the σ-complex, phenylacetylene is coordinated to the ruthenium center in an η^2 manner with the σ-electrons of the C1−H1 bond of phenylacetylene. The C1−C2, Ru−C1, and Ru−H1 distances in **2_d** are 1.247, 2.036, and 1.754 Å, respectively. In the π-complex (**2_c**), phenylacetylene is coordinated to the ruthenium center in an η^2 fashion. The relaxed surface scans also suggest the occurrence of the σ-complex instead of the π-complex. Additionally, from the thermodynamic standpoint, the appearance of the π-complex in the reaction profile is less probable. The greater stabilization of the σ-complex can be attributed to the less steric interaction on phenylacetylene compared to that in the π-complex by the large phenyl rings of phosphine ligands. Hence the relevant σ-complex readily forms instead of the π-complex. The σ-complex is formed from **2_b** via an activation barrier of 24.47 kcal/mol. In **2_TS-b_d** geometry, the Ru−C1 and Ru−H1 distances are 2.581 and 2.262 Å, whereas the Ru−C2 distance is 3.683 Å, which is distinctly longer than the Ru−C1 distance.

The σ-complex can undergo a 1,2-hydrogen migration to form the ruthenium vinylidene complex (**2_e**). This 1,2-hydrogen migration step occurs via a small activation barrier of 6.03 kcal/mol. In the **2_TS-d_e** structure, the Ru−C1 bond distance again decreases to 1.957 Å and the C1−C2 distance increases to 1.281 Å compared to the distances in **2_d**. In **2_e**, the C1−C2 distance increases further to 1.341 Å and the Ru−C1 distance decreases to 1.804 Å. The vinylidene complex (**2_e**) is a thermodynamically stable intermediate. Also, the reaction energy suggests that **2_e** is more stable than **2_d** by $\Delta_r E_{tot}$ = 8.17 kcal/mol and $\Delta_r G_{298}$ = 4.30 kcal/mol. Therefore, this rearrangement is thermodynamically feasible. All the related geometries of catalyst **2** are given in Figure 6.

Addition of pyrazole to the ruthenium vinylidene complex occurs via an intermediate adduct **2_f**, in which pyrazole is noncovalently bound with the ruthenium vinylidene complex (**2_e**). Among the various possible orientations by which pyrazole can approach the metal center, two adducts were characterized (**2_f-*pro-cis*** and **2_f-*pro-trans***). Pyrazole-bound

dx.doi.org/10.1021/jo502151z | J. Org. Chem. 2014, 79, 9979−9991

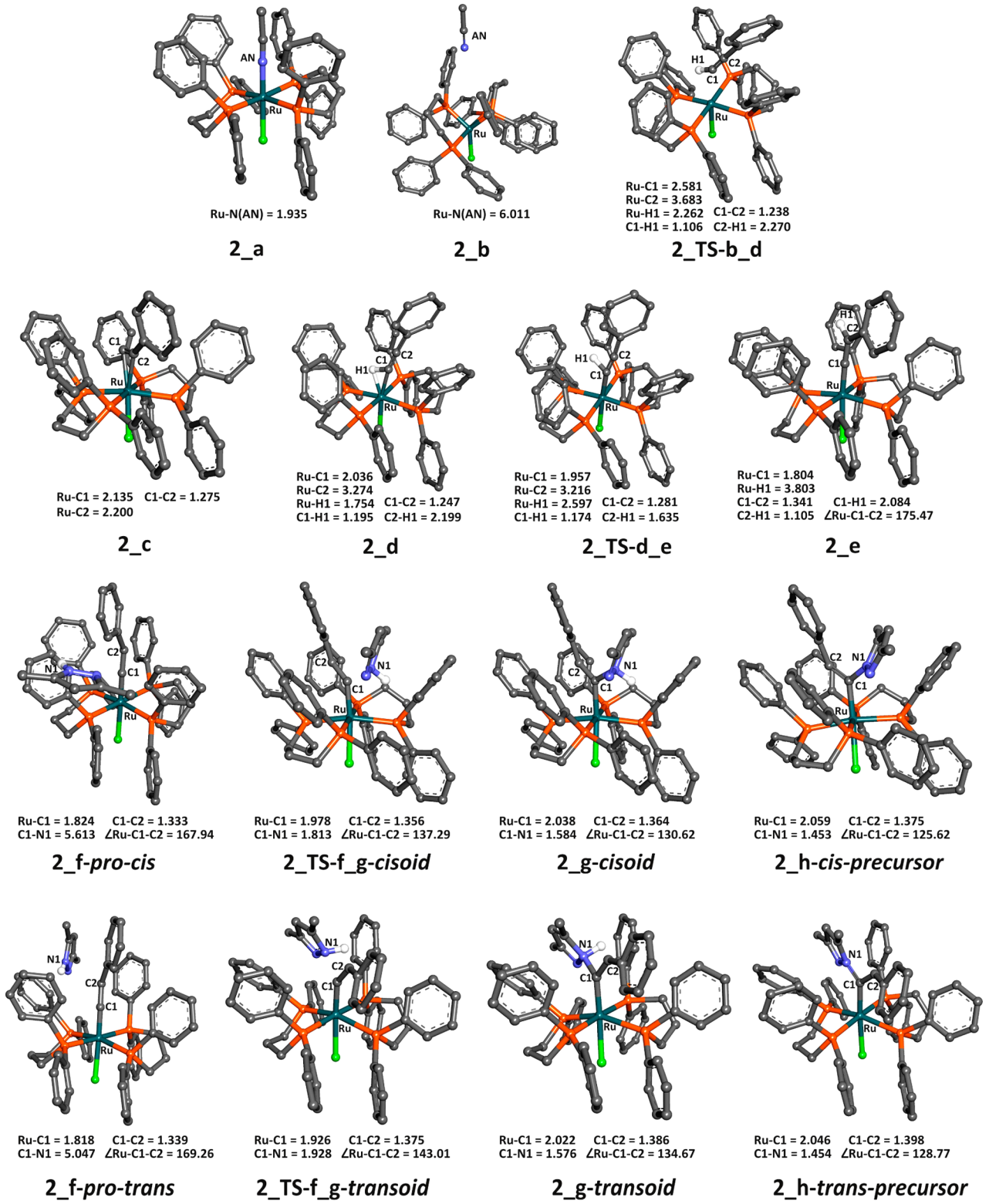

Figure 6. Geometries of the intermediates and transition states for the vinylation of pyrazole in the presence of **2**. Hydrogen atoms are not shown for clarity. Selected distances and angles are presented in angstroms and degrees, respectively.

complex **2_f** is more stable than **2_e** by $\Delta_r E_{tot} = -28.50$ kcal mol^{-1} and $\Delta_r G_{298} = -18.46$ kcal mol^{-1} for the related *pro-cis* orientation (**2_f-*pro-cis***) and by $\Delta_r E_{tot} = -15.62$ kcal mol^{-1} and $\Delta_r G_{298} = -5.53$ kcal mol^{-1} for the *pro-trans* orientation (**2_f-*pro-trans***). The **2_f-*pro-cis*** species is more stable than **2_f-*pro-trans*** by 10.09 kcal/mol. Stereoselection is initiated at this complex.

In the subsequent step, the N(H) center of the pyrazole attacks the carbon atom α to the ruthenium(II) center in anti-Markovnikov's fashion to generate **2_g** in *cisoid* and *transoid* forms. For the *pro-cis*orientation, the addition of pyrazole to the vinylidine carbon occurs with an activation barrier of $\Delta^{\ddagger}G_{298} = 42.26$ kcal/mol and $\Delta^{\ddagger}E_{tot} = 38.27$ kcal/mol. In the

dx.doi.org/10.1021/jo502151z | J. Org. Chem. 2014, 79, 9979−9991

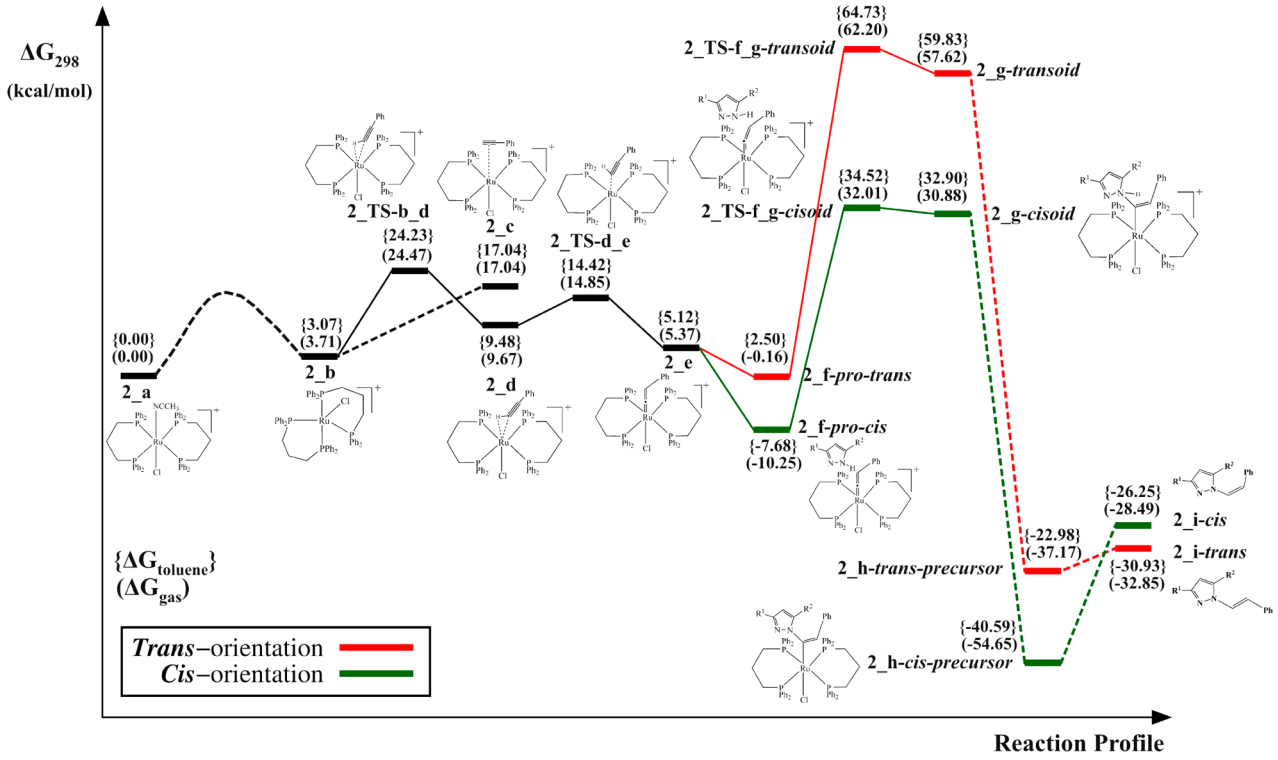

Figure 7. Energy profile for the vinylation of pyrazole in the presence of **2**. The values presented in parentheses are ΔG_{298} in the gas phase, and values in braces are ΔG_{298} in toluene.

2_TS-f_g-*cisoid* structure, the C1−N1 distance is 1.813 Å. However, for the related *pro-trans* orientation, the addition step demands a large barrier of $\Delta^{\ddagger}G_{298}$ = 62.36 kcal/mol and $\Delta^{\ddagger}E_{tot}$ = 57.31 kcal/mol. In the **2_TS-f_g-*transoid*** geometry, the C1−N1 distance is 1.928 Å, which is notably longer than the **2_TS-f_g-*cisoid*** geometry.

The large difference between the two activation barriers justifies the stereospecific production of *cisoid* geometry. The energy at this step is also stereogenic toward the selective formation of the *cisoid* intermediate. The **2_g_*cisoid*** species is more stable than **2_g_*transoid*** by 26.64 kcal/mol ($\Delta_r G_{298}$).

In the following step, removal of one proton produces the related *cis*- (**2_h_*cis-precursor***) and *trans*-precursors (**2_g_*trans-precursor***). This step is highly exothermic and exergonic for both the *cis*- ($\Delta_r E_{tot}$ = −80.93 kcal/mol and $\Delta_r G_{298}$ = −85.53 kcal/mol) and *trans*-precursor geometry ($\Delta_r E_{tot}$ = −87.64 kcal/mol and $\Delta_r G_{298}$ = −94.79 kcal/mol). Between the **2_h** geometries, the **2_h_*cis-precursor*** is more stable than **2_h_*trans-precursor*** by 17.48 kcal/mol, making *cis* the obvious choice for the product stereochemistry. The free energy profile for the catalytic cycle is shown in Figure 7. The large energy differences between **2_TS-f_g-*cisoid*** and **2_TS-f_g-*transoid*** translate to the selectivity for the *cis* isomeric product. Protonolysis of **2_h_*cis-precursor*** produces *cis*-(*Z*) and **2_h_*trans-precursor*** produces *trans*-(*E*) products.

It is clear from the optimized geometry of the ruthenium species **1_e** that it has a sterically less hindered reaction site and the *trans*-substituent of the alkenyl group can be easily accommodated, thus leading to the formation of *trans*-alkenyl product, which is also thermodynamically more favorable than the corresponding *cis*-alkenyl product. In contrast, the optimized geometry of the ruthenium species **2_e** shows that the reaction site is surrounded by four PPh_2 groups and prevents the formation of the *trans*-alkenyl product, leading to the formation of the *cis*-alkenyl product, which is thermodynamically less stable with respect to the olefin geometry.

CONCLUSION

In conclusion, it has been shown that the ruthenium complexes $[Ru(dppe)(PPh_3)(CH_3CN)_2Cl][BPh_4]$ (**1**) and $[Ru(dppp)_2(NCCH_3)Cl][BPh_4]$ (**2**) are efficient catalysts for regio- and stereoselective addition of pyrazoles to alkynes, and the stereoselectivity is dependent upon the ligand environment around the ruthenium center.

EXPERIMENTAL SECTION

Solvents and reagents used were reagent grade products. ^{1}H NMR, ^{13}C NMR, and NOESY spectra were recorded on 400 and 200 MHz (^{1}H frequency) spectrometers. HRMS data of the newly synthesized compounds were recorded on TOF MS in ESI+ mode in a methanol−water mixture. Complexes **1** and **2** have been synthesized by the procedure reported from this laboratory.[12,13]

Single-Crystal Data Collection and Refinements. Single-crystal X-ray data of 2-[3-(3-methyl-5-phenyl-1*H*-pyrazol-1-yl)allyl)-isoindoline-1,3-dione (**6z**) were collected on a single-crystal X-ray diffractometer that uses graphite monochromated Mo Kα radiation (λ = 0.71073 Å). The structure was solved by direct methods and refined by the least-square method on F^2 employing the WinGx[22a] package and the relevant programs (SHELX-97[23] and ORTEP-3[22b]) implemented therein. Non-hydrogen atoms were refined anisotropically, and hydrogen atoms on C atoms were fixed at calculated positions and refined using a riding model.

Computational Details. All the computations were performed with the Turbomole V6.5[24] software package. All optimizations of the ground-state geometries were done in the gas phase using the DFT method BP86[25,26] with resolution of the identity (RI[27]) approximation. The def2-SVP[28] basis set and the corresponding auxiliary basis set were used for all calculations. Restricted approach was used in the computational analysis for the closed shell structures. For ruthenium atoms, the effective core potential[29] was taken into account. Grimme's

dx.doi.org/10.1021/jo502151z | J. Org. Chem. 2014, 79, 9979−9991

empirical dispersion correction D3[30] with BJ[31] (D3-BJ) was included in all calculations. The characteristics of the stationary points were characterized by vibrational frequency calculation. All ΔG values are calculated at 298 K. Single-point calculations were done with B3LYP[32](D3-BJ)/def2-SVP level of theory on BP86-optimized geometries. Solvent effects by the solvent toluene (ε = 2.38) were considered by single-point calculations at BP86(RI,D3-BJ)/def2-SVP level with the COSMO[33] (the conductor-like screening model).

[Ru(dppe)$_2$(CH$_3$CN)Cl][BPh$_4$] (1) and [Ru(dppp)$_2$(CH$_3$CN)Cl][BPh$_4$] (2) Catalyzed Reaction of Alkynes with Pyrazole. The alkyne (1.0 mmol) and either **1** or **2** (0.005 mmol) and toluene (5 cm^3) were taken in a round-bottomed flask fitted with a refluxing condenser along with a stirring bar. To this was added pyrazole (1 mmol), and the reaction solution was heated in an oil bath for 5−8 h. The reaction solution was cooled to room temperature, and solvent and other volatile components were removed under vacuum. The resulting products were purified by column chromatography using silica gel 60−120 and 100−200 mesh using a mixture of hexane and ethyl acetate (2%) as eluent. Structural assignments of the products were made on the basis 1D and 2D NMR techniques. The spectra are given in the Supporting Information. The single-crystal X-ray structure of one of the products, namely, (*E*)-2-[5-(3,5-dimethylpyrazol-1-yl)pent-4-en-1-yl]isoindole-1,3-dione (**5f**), has been determined and reported in our earlier recent communication.[12]

*(Z)-1-Styryl-1H-pyrazole (**6a**):* A pale yellow oil, 98% yield (0.167 g); ^{1}H NMR (200 MHz, CDCl$_3$, ppm) δ 6.17 (t, J = 2.0 Hz, 1H), 6.2 (d, J = 9.8 Hz, 1H), 6.98 (d, J = 9.8 1H), 7.16 (d, J = 1.6 Hz, 1H), 7.18−7.20 (m, 2H), 7.24−7.29 (m, 3H), 7.58 (d, J = 1.4 Hz, 1H); ^{13}C NMR (50 MHz, CDCl$_3$, ppm) δ 106.7, 119.0, 127.0, 127.9, 128.6, 128.7, 129.5, 134.4, 140.3; HRMS (ESI) calcd for C$_{11}$H$_{11}$N$_2$ [M + H]$^+$ 171.0917, found 171.0910.

*(Z)-1-[2-(4-Fluorophenyl)vinyl]-1H-pyrazole (**6b**):* A pale yellow oil, 95% yield (0.179 g); ^{1}H NMR (200 MHz, CDCl$_3$, ppm) δ 6.20−6.24 (m, 2H), 6.95−7.03 (m, 3H), 7.13−7.20 (m, 2H), 7.29 (d, J = 2.2 Hz, 1H), 7.60 (d, J = 1.2 Hz, 1H); ^{13}C NMR (50 MHz, CDCl$_3$, ppm) δ 106.9, 115.5, 116.0, 118.7, 127.0, 129.6, 130.6, 130.7, 140.5, 159.9, 164.8; HRMS (ESI) calcd for C$_{11}$H$_{10}$FN$_2$ [M + H]$^+$ 189.0823, found 189.0828.

*(Z)-1-[2-(4-Methoxyphenyl)vinyl]-1H-pyrazole (**6c**):* A pale yellow oil, 95% yield (0.192 g); ^{1}H NMR (400 MHz, CDCl$_3$, ppm) δ 3.79 (s, 3H), 6.20−6.23 (m, 2H), 6.81 (d, J = 8.8 Hz, 2H), 6.90 (d, J = 9.2 Hz, 1H), 7.08 (d, J = 8.8 Hz, 2H), 7.36 (d, J = 2.4 Hz 1H), 7.59 (s, 1H); ^{13}C NMR (100 MHz, CDCl$_3$, ppm) δ 55.4, 106.7, 114.2, 120.1, 125.9, 127.6 129.7, 130.2, 140.3, 159.4; HRMS (ESI) calcd for C$_{12}$H$_{13}$N$_2$O [M + H]$^+$ 201.1028, found 201.1030.

*(Z)-1-Hex-1-enyl-1H-pyrazole (**6d**):* A colorless oil, 87% yield (*E*/*Z* mixture 0.131 g); ^{1}H NMR (400 MHz, CDCl$_3$, ppm) δ 0.85−0.97 (m, 3H), 1.13−1.38 (m, 2H), 1.41−1.57 (m, 2H), 2.40 (quint, J = 7.2 Hz, 2H), 5.22 (dt, J = 9.2, 7.2 Hz, 1H), 6.31 (m, 1H), 6.76 (d, J = 9.6 Hz), 7.52 (d, J = 1.2 Hz, 1H), 7.60 (s, 1H); ^{13}C NMR (50 MHz, CDCl$_3$, ppm) δ 14.2, 22.5, 27.0, 31.9, 106.2, 121.6, 126.1, 129.9, 140.1; HRMS (ESI) calcd for C$_9$H$_{15}$N$_2$ [M + H]$^+$ 151.1165, found 151.1153.

*(E)-1-Hex-1-enyl-1H-pyrazole (**6d**):* A colorless oil, 87% yield; ^{1}H NMR (400 MHz, CDCl$_3$, ppm) δ 0.85−0.97 (m, 3H), 1.13−1.38 (m, 2H), 1.41−1.57 (m, 2H), 2.14 (quint, J = 7.2 Hz, 2H), 6.04 (dt, J = 14.0, 7.2 Hz, 1H), 6.30 (m, 1H), 6.83 (d, J = 14.0 Hz), 7.54 (d, J = 1.0 Hz, 1H), 7.56 (s, 1H); ^{13}C NMR (50 MHz, CDCl$_3$, ppm) δ 14.2, 22.3, 27.0, 31.7, 106.6, 118.4, 127.2, 129.9, 140.3; HRMS (ESI) calcd for C$_9$H$_{15}$N$_2$ [M + H]$^+$ 151.1165, found 151.1153.

*(Z)-1-Oct-1-enyl-1H-pyrazole (**6e**):* A colorless oil, 85% yield (*E*/*Z* mixture 0.151 g); ^{1}H NMR (200 MHz, CDCl$_3$, ppm) δ 0.84- 0.90 (m, 3H), 1.25−1.49 (m, 8H), 2.36 (q, J = 7.0 Hz, 2H), 5.18 (dt, J = 9.2, 7.2 Hz, 1H), 6.31 (t, J = 2.2 Hz, 1H), 6.75 (d, J = 9.6, Hz, 1H), 7.51 (m, 1H), 7.59 (s, 1H); ^{13}C NMR (50 MHz, CDCl$_3$) δ 14.2, 22.7, 27.3, 29.0, 29.7, 31.8, 106.1, 121.6, 126.0, 129.9, 140.1; HRMS (ESI) calcd for C$_{11}$H$_{19}$N$_2$ [M + H]$^+$ 179.1549, found 179.1541.

*(E)-1-Oct-1-enyl-1H-pyrazole (**6e**):* A colorless oil, 85% yield; ^{1}H NMR (200 MHz, CDCl$_3$, ppm) δ 0.84−0.90 (m, 3H), 1.25−1.49 (m, 8H), 2.10 (q, J = 6.8 Hz, 2H), 5.99 (dt, J = 7.4, 7.0 Hz, 1H), 6.29 (t, J = 2.2 Hz, 1H), 6.80 (d, J = 16.6 Hz, 1H), 7.51 (m, 1H), 7.58 (s, 1H); ^{13}C NMR (50 MHz, CDCl$_3$) δ 14.2, 22.7, 27.3, 29.7, 29.5, 31.8, 106.5, 118.4, 127.1, 129.9, 140.3.

*(Z)-1-(3-Phenoxypropenyl)-1H-pyrazole (**6f**):* A pale yellow oil, 90% yield (0.2 g); ^{1}H NMR (200 MHz, CDCl$_3$, ppm) δ 5.17 (dd, J = 5.6, 1.8 Hz, 2H), 5.44 (dt, J = 9.6, 5.6 Hz, 1H), 6.36 (t, J = 2.0 Hz, 1H), 6.83 (d, J = 9.6 Hz, 1H), 6.92−6.99 (m, 3H), 7.25−7.33(m, 2H), 7.55 (d, J = 2.2 Hz, 1H), 7.69 (s, 1H); ^{13}C NMR (50 MHz, CDCl$_3$) δ 64.7, 106.9, 114.9, 115.3, 121.0, 126.1, 129.6, 130.5, 141.5, 158.5; HRMS (ESI) calcd for C$_{12}$H$_{13}$N$_2$O [M + H]$^+$ 201.1028, found 201.1030.

*(Z)-2-(3-Pyrazol-1-ylallyl)isoindole-1,3-dione (**6g**):* A white solid, 87% yield (0.22 g); ^{1}H NMR (400 MHz, CDCl$_3$) δ 4.95 (dd, J = 6.0, 1.6 Hz, 2H), 5.14 (dt, J = 9.6, 1.6 Hz, 1H), 6.36 (t, J = 2.0 Hz, 1H), 6.77 (dt, J = 9.6, 5.6, Hz, 1H), 7.63 (d, J = 2.4 Hz, 1H), 7.68 (s, 1H), 7.70−7.73(m, 2H), 7.83−7.85 (m, 2H); ^{13}C NMR (100 MHz, CDCl$_3$) δ 36.0, 106.1, 113.7, 123.5, 126.6, 130.7, 133.0, 134.2, 141.4, 168.2; HRMS (ESI) calcd for C$_{14}$H$_{12}$N$_3$O$_2$ [M + H]$^+$ 254.0924, found 254.0922.

*(Z)-2-(5-Pyrazol-1-ylpent-4-enyl)isoindole-1,3-dione (**6h**):* A white solid, 83% yield (0.233 g); ^{1}H NMR (200 MHz, CDCl$_3$) δ 1.78 (quint, J = 7.4 Hz, 2H), 2.51 (q, J = 7.4 Hz, 2H), 3.68 (t, J = 7.4 Hz, 2H), 5.18 (dt, J = 8.8, 7.4 Hz, 1H), 6.28 (s, 1H), 6.72 (dd, J = 9.2, 8.4 Hz, 1H), 7.47(m, 2H), 7.66−7.69 (m, 2H), 7.71−7.77 (m, 2H); ^{13}C NMR (50 MHz, CDCl$_3$) δ 24.5, 28.4, 37.5, 106.1, 119.1, 123.2, 126.3, 130.0, 132.1, 133.9, 140.2, 168.4; HRMS (ESI) calcd for C$_{16}$H$_{16}$N$_3$O$_2$ [M + H]$^+$ 282.1237, found 282.1235.

*(Z)-3-Methyl-1-styryl-1H-pyrazole (**6i**):* A colorless oil, 92% yield (0.17 g); ^{1}H NMR (400 MHz, CDCl$_3$) δ 2.30 (s, 3H), 5.96 (d, J = 2.0 Hz, 1H), 6.14 (d, J = 9.6 Hz, 1H), 6.93 (d, J = 9.6 Hz, 1H), 7.18 (d, J = 2.0 Hz, 1H) 7.21−7.32 (m, 5H); ^{13}C NMR (100 MHz, CDCl$_3$) δ 13.6,106.7, 117.6, 127.0, 127.8, 128.7, 128.8, 130.3, 134.8, 149.7; HRMS (ESI) calcd for C$_{12}$H$_{13}$N$_2$ [M + H]$^+$ 185.1073, found 185.1090.

*(Z)-3,5-Dimethyl-1-styryl-1H-pyrazole (**6j**):* A white solid, 95% yield (0.168 g); ^{1}H NMR (200 MHz, CDCl$_3$, ppm) δ 1.89 (s, 3H), 2.27 (s, 3H), 5.8 (s, 1H), 6.42 (d, J = 8.8 Hz, 1H), 6.70 (d, J = 8.8 Hz, 1H), 6.95−7.00 (m, 2H), 7.19−7.22 (m, 3H); ^{13}C NMR (100 MHz, CDCl$_3$) δ 11.2, 13.6, 105.9, 124.6, 127.4, 128.1, 128.3, 128.7, 134.2, 139.9, 149.5; HRMS (ESI) calcd for C$_{13}$H$_{15}$N$_2$ [M + H]$^+$ 199.1230, found 199.1236.

*(Z)-1-[2-(4-Fluorophenyl)vinyl]-3,5-dimethyl-1H-pyrazole (**6k**):* An orange oil, 94% yield (0.203 g); ^{1}H NMR (200 MHz, CDCl$_3$, ppm) δ 1.39 (s, 3H), 2.25 (s, 3H), 5.85 (s, 1H), 6.36 (d, J = 9.0 Hz, 1H), 6.67 (d, J = 9.0 Hz, 1H), 6.85−7.01 (m, 4H); ^{13}C NMR (50 MHz, CDCl$_3$, ppm) δ 11.2, 13.7, 106.2, 115.2, 115.6, 124.3, 130.4, 130.7, 130.8, 139.9, 149.7; HRMS (ESI) calcd for C$_{13}$H$_{14}$FN$_2$ [M + H]$^+$ 217.1136, found 217.1135.

*(Z)-1-[2-(4-Methoxyphenyl)vinyl]-3,5-dimethyl-1H-pyrazole (**6l**):* A yellow solid, 95% yield (0.216 g); ^{1}H NMR (400 MHz, CDCl$_3$, ppm) δ 1.93 (s, 3H), 2.27 (s, 3H), 3.76 (s, 3H), 5.85 (s, 1H), 6.38 (d, J = 8.8 Hz, 1H), 6.60 (d, J = 8.8 Hz, 1H), 6.72 (d, J = 8.8 Hz, 2H), 6.88 (d, J = 8.8 Hz, 2H); ^{13}C NMR (100 MHz, CDCl$_3$, ppm) δ 11.3, 13.8, 55.3, 106.0, 114.0, 123.0, 126.9, 127.9, 13.4, 140.1, 149.5, 159.6; HRMS (ESI) calcd for C$_{14}$H$_{17}$N$_2$O [M + H]$^+$ 229.1335, found 229.1336.

*(Z)-1-(2-Cyclohexylvinyl)-3,5-dimethyl-1H-pyrazole (**6m**):* A colorless oil, 82% yield (0.176 g); ^{1}H NMR (400 MHz, CDCl$_3$, ppm) δ 1.61−1.81(m, 9H), 2.19 (s, 3H), 2.24 (s, 3H), 2.81(m 1H), 5.16 (t, J = 9.2 Hz, 1H), 5.82 (s, 1H), 6.35 (d, J = 8.8 Hz, 1H); ^{13}C NMR (100 MHz, CDCl$_3$, ppm) δ 11.4, 13.8, 25.8, 26.2, 33.0, 35.6, 105.2, 121.3, 1310.3, 138.3, 149.3; HRMS (ESI) calcd for C$_{13}$H$_{21}$N$_2$ [M + H]$^+$ 205.1705, found 205.1705.

*(Z)-1-Hex-1-enyl-3,5-dimethyl-1H-pyrazole (**6n**):* A colorless oil, 81% yield (*E*/*Z* mixture 0.144 g); ^{1}H NMR (400 MHz, CDCl$_3$, ppm) δ 0.83−0.90 (m, 3H). 1.27−1.46 (m, 4H), 2.21 (s, 6H), 2.35 (q, J = 7.2 Hz, 2H), 5.31 (q, J = 7.6 Hz, 1H), 5.79 (s, 1H), 6.44 (d, J = 9.2 Hz, 1H); ^{13}C NMR (100 MHz, CDCl$_3$, ppm) δ 11.3, 13.7, 22.3, 26.7, 31.6, 105.1, 123.1, 125.8, 139.6, 148.5; HRMS (ESI) calcd for C$_{11}$H$_{19}$N$_2$ [M + H]$^+$ 179.1543, found 179.1550.

*(E)-1-Hex-1-enyl-3,5-dimethyl-1H-pyrazole (**6n**):* A colorless oil, 81% yield; ^{1}H NMR (400 MHz, CDCl$_3$, ppm) δ 0.83−0.90 (m, 3H). 1.27−1.46 (m, 4H), 2.11−2.21 (m, 2H), 2.16 (s, 6H), 5.79 (s, 1H), 6.08−6.16 (m, 1H), 6.59 (d, J = 13.2 Hz, 1H); ^{13}C NMR (100 MHz, CDCl$_3$, ppm) δ 11.0, 13.6, 22.2, 30.0, 31.8, 106.1, 118.4, 123.4, 138.4, 149.1; HRMS (ESI) calcd for C$_{11}$H$_{19}$N$_2$ [M + H]$^+$ 179.1543, found 179.1550.

dx.doi.org/10.1021/jo502151z | J. Org. Chem. 2014, 79, 9979−9991

*(Z)-3,5-Dimethyl-1-oct-1-enyl-1H-pyrazole (**6o**):* A colorless oil, 80% yield (*E*/*Z* mixture 0.165 g); ^{1}H NMR (200 MHz, $CDCl_3$) δ 0.86−0.87 (m, 3H), 1.25−1.41 (m, 8H), 2.20 (s, 6H), 2.34 (q, *J* = 6.6 Hz, 2H), 5.30 (dt, *J* = 8.6, 7.4 Hz, 1H), 5.82 (s, 1H), 6.45 (d, *J* = 8.8 Hz, 1H); ^{13}C NMR (50 MHz, $CDCl_3$) δ 11.4, 13.8, 14.2, 22.7, 27.1, 29.0, 29.5, 31.8, 105.2, 123.1, 125.9, 139.7, 148.6; HRMS (ESI) calcd for $C_{13}H_{23}N_2$ $[M + H]^+$ 207.1856, found 207.1860.

*(E)-3,5-Dimethyl-1-oct-1-enyl-1H-pyrazole (**6o**):* A colorless oil, ^{1}H NMR (200 MHz, $CDCl_3$) δ 0.86−0.87 (m, 3H), 1.25−1.41 (m, 8H), 2.1(m, 2H) 2.18 (s, 6H), 5.82 (s, 1H), 6.07 (m, 1H), 6.59 (d, *J* = 13.8 Hz, 1H); ^{13}C NMR (50 MHz, $CDCl_3$) δ 11.2, 13.8, 14.2, 22.7, 27.1, 29.0, 29.8, 31.9, 106.2, 123.5, 125.9, 138.5, 149.2; HRMS (ESI) calcd for $C_{13}H_{23}N_2$ $[M + H]^+$ 207.1856, found 207.1860.

*(Z)-3,5-Dimethyl-1-(3-phenoxypropenyl)-1H-pyrazole (**6p**):* A pale yellow oil, 80% yield (0.231 g); ^{1}H NMR (200 MHz, $CDCl_3$, ppm) δ 2.18 (s, 6H), 5.14 (dd, *J* = 7.6, 1.2 Hz, 2H), 5.25 (dt, *J* = 9.2, 7.41 H), 5.80 (s, 1H), 6.52 (d, *J* = 9.4 Hz, 1H), 6.81−6.95 (m, 3H), 7.15−7.27 (m, 2H); ^{13}C NMR (50 MHz, $CDCl_3$) δ 11.3, 13.9, 65.1, 106.4, 115.0, 115.1, 120.7, 122.6, 129.6, 140.0, 149.9, 158.7; HRMS (ESI) calcd for $C_{14}H_{17}N_2O$ $[M + H]^+$ 229.1335, found 229.1338.

*(Z)-3,5-Dimethyl-1-[2-(4-phenoxyphenyl)vinyl]-1H-pyrazole (**6q**):* A yellow oil, 86% yield (0.25 g); ^{1}H NMR (200 MHz, $CDCl_3$, ppm) δ 1.98 (s, 3H), 2.26 (s, 3H), 5.86 (s, 1H), 6.38 (d, *J* = 9.0 Hz, 1H), 6.69 (d, *J* = 9.0 Hz, 1H), 6.82−6.86 (m, 2H), 6.94−7.11 (m, 4H), 7.29−7.37 (m, 3H); ^{13}C NMR (50 MHz, $CDCl_3$, ppm) δ 11.2, 13.6, 105.9, 118.2, 119.3,123.6, 126.9, 129.0, 129.8, 130.4, 139.8, 149.4, 156.6, 157.3; HRMS (ESI) calcd for $C_{19}H_{19}N_2O$ $[M + H]^+$ 291.1492, found 291.1490.

*(Z)-3,4,5-Trimethyl-1-styryl-1H-pyrazole (**6r**):* A colorless oil, 92% yield (0.195 g); ^{1}H NMR (200 MHz, $CDCl_3$, ppm) δ 1.82 (s, 3H), 1.88 (s, 3H), 2.21 (s, 3H), 6.35 (d, *J* = 9.0 Hz, 1H), 6.69 (d, *J* = 9.0 Hz, 1H), 6.97−7.02 (m, 2H), 7.16−7.21 (m, 3H); ^{13}C NMR (50 MHz, $CDCl_3$, ppm) δ 8.2, 10.0, 12.1, 112.6, 124.9, 126.4, 128.0, 128.4, 128.9, 134.6, 136.7, 148.6; HRMS (ESI) calcd for $C_{14}H_{17}N_2$ $[M + H]^+$ 213.1386, found 213.1391.

*(Z)-3-Methyl-5-phenyl-1-styryl-1H-pyrazole (**6s**):* A yellow oil, 86% yield (0.224 g); ^{1}H NMR (400 MHz, $CDCl_3$, ppm) δ 2.34 (s, 3H), 6.19 (s, 1H), 6.32 (d, *J* = 8.8 Hz, 1H), 6.75 (d, *J* = 8.8 Hz, 1H), 6.91−6.93 (m, 2H), 7.12−7.15 (m, 3H), 7.26−7.27 (m, 5H); ^{13}C NMR (100 MHz, $CDCl_3$, ppm) δ 13.8, 106.6, 125.1, 127.0, 127.9, 128.1, 128.2, 128.3, 128.4, 129.1, 130.3, 134.1, 144.8, 149.7; HRMS (ESI) calcd for $C_{18}H_{17}N_2$ $[M + H]^+$ 261.1386, found 261.1389.

*(Z)-3-Methyl-1-(3-phenoxypropenyl)-5-phenyl-1H-pyrazole (**6t**):* A yellow oil, 80% yield (0.232 g); ^{1}H NMR (400 MHz, $CDCl_3$, ppm) δ 2.36 (s, 3H), 5.24 (dd, *J* = 5.2, 1.6 Hz, 2H), 5.37 (dt, *J* = 9.2, 5.6 Hz, 1H), 6.19 (s, 1H), 6.67 (dt, *J* = 9.2, 2.0 Hz, 1H), 6.92−6.99 (m, 3H), 7.28−7.20 (m, 2H), 7.39−7.46 (m, 5H); ^{13}C NMR (50 MHz, $CDCl_3$, ppm) δ 14.0, 65.1, 106.9, 114.9, 115.9, 120.8, 124.3, 128.8, 129.2, 129.6, 145.1, 150.2, 158.7; HRMS (ESI) calcd for $C_{19}H_{19}N_2O$ $[M + H]^+$ 291.1492, found 291.1497.

*(Z)-1-Hex-1-enyl-3,5-diphenyl-1H-pyrazole (**6u**):* A pale yellow oil, 77% yield (*E*/*Z* mixture 0.156 g); ^{1}H NMR (400 MHz, $CDCl_3$, ppm) δ 0.88−0.93 (m, 3H), 1.39−1.47 (m, 4H), 2.50 (q, *J* = 7.2 Hz, 2H), 5.36 (dt, *J* = 8.8, 7.6 Hz, 1H), 6.64 (d, *J* = 8.8 Hz, 1H), 6.70 (s, 1H), 7.38−7.52 (m, 8H), 7.78 (d, *J* = 7.6, 2H); ^{13}C NMR (100 MHz, $CDCl_3$, ppm) δ 14.1, 22.7, 27.2, 31.6, 103.4, 124.2, 125.6, 125.8, 126.0, 128.0, 128.7, 129.1, 129.5, 130.6, 133.4, 145.2, 151.3; HRMS (ESI) calcd for $C_{21}H_{23}N_2$ $[M + H]^+$ 303.1856, found 303.1860.

*(E)-1-Hex-1-enyl-3,5-diphenyl-1H-pyrazole (**6u**):* A pale yellow oil, 77% yield; ^{1}H NMR (400 MHz, $CDCl_3$, ppm) δ 0.88−0.93 (m, 3H), 1.39−1.47 (m, 4H), 2.13 (q, *J* = 6.8 Hz, 2H), 6.40 (m, 1H), 6.70 (s, 1H), 6.77 (d, *J* = 14.0 Hz, 1H), 7.31−7.34 (m, 8H), 7.73 (d, *J* = 7.6, 2H); ^{13}C NMR (100 MHz, $CDCl_3$, ppm) δ 14.1, 22.4, 30.0, 31.8, 104.4, 120.6, 124.6, 125.8, 126.0, 128.7, 128.9, 129.1, 129.5, 130.6, 133.4, 145.2, 151.3; HRMS (ESI) calcd for $C_{21}H_{23}N_2$ $[M + H]^+$ 303.1856, found 303.1860.

*(Z)-3,5-Diphenyl-1-styryl-1H-pyrazole (**6v**):* A white solid, 85% yield (0.274 g); ^{1}H NMR (200 MHz, $CDCl_3$, ppm) δ 6.37 (d, *J* = 9.2 Hz, 1H), 6.71 (s, 1H), 6.85 (d, *J* = 9.0 Hz, 1H), 7.02−7.07 (m, 2H), 7.15−7.19 (m, 3H), 7.29−7.45 (m, 8H), 7.81−7.85 (m, 2H); ^{13}C NMR (50 MHz, $CDCl_3$, ppm) δ 104.1, 124.9, 125.9, 126.8, 128.0, 128.2, 128.5, 128.7, 128.8, 129.2, 130.2, 133.1, 134.2, 145.5, 152.0; HRMS (ESI) calcd for $C_{23}H_{19}N_2$ $[M + H]^+$ 323.1543, found 323.1550.

*(Z)-2-[5-(3,5-Dimethylpyrazol-1-yl)-pent-4-enyl]isoindole-1,3-dione (**6w**):* A white solid, 85% yield (0.263 g); ^{1}H NMR (400 MHz, $CDCl_3$, ppm) δ 1.78−1.86 (m, 2H), 2.12 (s, 3H), 2.18 (s, 3H), 2.53 (quint, *J* = 7.6 Hz, 2H), 3.67 (t, *J* = 7.6 Hz, 2H), 5.25 (dt, *J* = 8.8, 7.6 Hz, 1H), 5.76 (s, 1H), 6.47 (d, *J* = 9.2 Hz, 1H), 7.66−7.68 (m, 2H), 7.79−7.81 (m, 2H); ^{13}C NMR (50 MHz, $CDCl_3$, ppm) δ 11.4, 13.7, 24.4, 28.3, 37.7, 105.5, 121.5, 123.3, 123.5, 132.3, 133.9, 139.8, 148.9, 168.5; HRMS (ESI) calcd for $C_{18}H_{20}N_3O_2$ $[M + H]^+$ 310.1550, found 310.1557.

*(Z)-2-[5-(3,4,5-Trimethylpyrazol-1-yl)pent-4-enyl]isoindole-1,3-dione (**6x**):* A white solid, 80% yield (0.258 g); ^{1}H NMR (200 MHz, $CDCl_3$, ppm) δ 1.78 (m, 2H), 1.86 (s, 3H), 2.07 (s, 3H), 2.10 (s, 3H), 2.53 (quint, *J* = 7.4 Hz, 2H), 3.65 (t, *J* = 7.4 Hz, 2H), 5.16 (dt, *J* = 9.0,7.4 Hz, 1H), 6.47 (d, *J* = 9.0 Hz, 1H), 7.65−7.72 (m, 2H), 7.76−7.82 (m, 2H); ^{13}C NMR (50 MHz, $CDCl_3$, ppm) δ 7.9. 9.6. 11.9, 24.3, 28.1, 37.5, 120.3, 123.0, 123.5, 132.1, 133.7, 136.1, 147.8, 168.3; HRMS (ESI) calcd for $C_{19}H_{22}N_3O_2$ $[M + H]^+$ 324.1707, found 324.1713.

*(Z)-2-[3-(3,5-Dimethylpyrazol-1-yl)allyl]isoindole-1,3-dione (**6y**):* A white solid, 81% yield (0.228 g); ^{1}H NMR (400 MHz, $CDCl_3$, ppm) δ 2.24 (s, 3H), 2.25 (s, 3H), 4.99 (dd, *J* = 5.6, 1.6 Hz, 2H), 5.06 (dt, *J* = 9.2, 5.2 Hz, 1H), 5.85 (s, 1H), 6.56 (dt, *J* = 9.2, 1.6 Hz, 1H), 7.69−7.17 (m, 2H), 7.83−7.87 (m, 2H); ^{13}C NMR (100 MHz, $CDCl_3$, ppm) δ 11.3,13.9, 36.3, 106.3, 113.3, 123.4, 132.4, 134.0, 139.9, 149.8, 168.3; HRMS (ESI) calcd for $C_{16}H_{16}N_3O_2$ $[M + H]^+$ 282.1237, found 282.1241.

*(Z)-2-[3-(3,5-Dimethylpyrazol-1-yl)allyl]isoindole-1,3-dione (**6z**):* A white crystalline solid, 78% yield (0.267 g); ^{1}H NMR (400 MHz, $CDCl_3$, ppm) δ 2.35 (s, 3H), 5.03 (dd, *J* = 6.0, 1.6 Hz, 2H), 5.10 (dt, *J* = 8.8, 5.2 Hz, 1H), 6.18 (s, 1H), 6.61 (dt, *J* = 8.8, 1.6 Hz, 1H),7.38−7.43 (m, 5H), 7.70−7.73 (m, 2H), 7.84−7.87 (m, 2H); ^{13}C NMR (100 MHz, $CDCl_3$, ppm) δ 14.0, 36.4, 106.8, 114.3, 123.4, 125.2, 128.8, 129.3, 130.3, 132.4, 134.1, 145.0, 149.9, 168.3; HRMS (ESI) calcd for $C_{21}H_{18}N_3O_2$ $[M + H]^+$ 344.1394, found 344.1389.

■ ASSOCIATED CONTENT

Supporting Information

ORTEP view of **6z**, cif file, ^{1}H and ^{13}C NMR spectra and NOESY spectra, and details of the results of the theoretical calculations. This material is available free of charge via the Internet at http://pubs.acs.org.

■ AUTHOR INFORMATION

Corresponding Authors

*E-mail: mxb@.iitkgp.ac.in.

*E-mail: anoop@chem.iitkgp.ernet.in.

Notes

The authors declare no competing financial interest.

■ ACKNOWLEDGMENTS

We thank Department of Science & Technology, Government of India, New Delhi, for single-crystal X-ray, NMR, and HPC facilities, and SERB, Government of India, New Delhi, for financial support. U.K.D. thanks the Council of Scientific & Industrial Research, New Delhi for the fellowship. S.M. thanks the University Grant Commission (UGC) for the fellowship. We thank reviewers for their helpful comments.

■ REFERENCES

(1) (a) Taillefer, M.; Ouali, A.; Renard, B.; Spindler, J.-F. *Chem.—Eur. J.* **2006**, *12*, 5301. (b) Bao, W.; Liu, Y.; Lv, X. *Synthesis* **2008**, *12*, 1911. (c) Ouali, A.; Laurent, R.; Caminade, A.-M.; Majoral, J.-P.; Taillefer, M. *J. Am. Chem. Soc.* **2006**, *128*, 15990. (d) Kaddouri, H.; Vicente, V.; Ouali, A.; Ouazzani, F.; Taillefer, M. *Angew. Chem., Int. Ed.* **2009**, *48*, 333. (e) Brustolin, F.; Castelvetro, V.; Ciardelli, F.; Ruggeri, G.; Colligiani, A. *J. Polym. Sci., A: Polym. Chem.* **2001**, *39*, 253.

(2) Ogata, M.; Matsumoto, H.; Shimizu, S.; Kida, S.; Shiro, M.; Tawara, K. *J. Med. Chem.* **1987**, *30*, 1348.
(3) (a) Lebedev, A. Y.; Izmer, V. V.; Kazyul'kin, D. N.; Beletskaya, I. P.; Voskoboynikov, A. Z. *Org. Lett.* **2002**, *4*, 623. (b) Dejli, J. R.; Legros, J.; Bolm, C. *Chem. Commun.* **2005**, 973.
(4) (a) Kizhnyaev, V. N.; Pokatilov, F. A.; Tsypina, N. A.; Ratovskii, G. V.; Vereshchagin, L. I.; Smirnov, A. I. *Russ. J. Org. Chem.* **2002**, *38*, 1056.
(5) (a) Fukudome, Y.; Naito, H.; Hata, T.; Urabe, H. *J. Am. Chem. Soc.* **2008**, *130*, 1820. (b) Martin, R.; Cuenca, A.; Buchwald, S. L. *Org. Lett.* **2007**, *9*, 5521. (c) Martin, R.; Larsen, C. H.; Cuenca, A.; Buchwald, S. L. *Org. Lett.* **2007**, *9*, 3379. (d) Shafir, A.; Lichtor, P. A.; Buchwald, S. L. *J. Am. Chem. Soc.* **2007**, *129*, 3490.
(6) (a) Liao, Q.; Wang, Y.; Zhang, L.; Xi, C. *J. Org. Chem.* **2009**, *74*, 6371. (b) Wang, Z.; Bao, W.; Jiang, Y. *Chem. Commun.* **2005**, 2849.
(7) Kabir, M. S.; Lorenz, M.; Namjoshi, O. A.; Cook, J. M. *Org. Lett.* **2010**, *12*, 464.
(8) Tanaka, N.; Hatanaka, M.; Watabe, Y. Japanese Patent Application 1026, 1993.
(9) Tsuchimoto, T.; Aoki, K.; Wagatsuma, T.; Suzuki, Y. *Eur. J. Org. Chem.* **2008**, 4035.
(10) Gooßen, L. J.; Rauhaus, J. E.; Deng, G. *Angew. Chem., Int. Ed.* **2005**, *44*, 4042.
(11) (a) Naskar, S.; Bhattacharjee, M. *J. Organomet. Chem.* **2005**, *690*, 5006. (b) Naskar, S.; Bhattacharjee, M. *Tetrahedron Lett.* **2007**, *48*, 465. (c) Naskar, S.; Bhattacharjee, M. *Tetrahedron Lett.* **2007**, *48*, 3367. (d) Tripathy, J.; Bhattacharjee, M. *Tetrahedron Lett.* **2009**, *50*, 4863. (e) Das, U. K.; Bhattacharjee, M. *J. Organomet. Chem.* **2012**, *700*, 78.
(12) Das, U. K.; Bhattacharjee, M. *Chem.—Eur. J.* **2012**, *18*, 5180.
(13) Das, U. K.; Bhattacharjee, M. *RSC Adv.* **2014**, *4*, 21964.
(14) Crystal data for **6z**: emperical formula $C_{21}H_{17}N_3O_2$, formula weight 343.38; monoclinic, $P21/n$, $Z = 4$, $a = 18.321(10)$ Å, $b = 7.322(4)$ Å, $c = 14.433(8)$ Å, $\beta = 109.457(17)°$, $V = 1825.5(17)$ Å^3, $\rho_{calcd} = 1.249$ Mg/m^3, λ (Mo Kα) = 0.71073 Å, 21565 measured, 6291 unique ($R_{int} = 0.1389$); $R1 = 0.0748$, $wR2 = 0.1492$.
(15) Smirnova, E. S.; Melekhova, A. A.; Gurzhiy, V. V.; Selivanov, S. I.; Krupenya, D. V.; Koshevoy, I. O.; Tunik, S. P. *Z. Anorg. Allg. Chem.* **2012**, *638*, 415.
(16) Jordan, R. W.; Khoury, P. R.; Goddard, J. D.; Tam, W. *J. Org. Chem.* **2004**, *69*, 8467.
(17) Naota, T.; Takaya, H.; Murahashi, S.-I. *Chem. Rev.* **1998**, *98*, 2599.
(18) Trost, B. M.; Toste, F. D.; Pinkerton, A. B. *Chem. Rev.* **2001**, *101*, 2067.
(19) Uchimaru, Y. *Chem. Commun.* **1999**, 1133.
(20) Olivan, M.; Clot, E.; Eisenstein, O.; Caulton, K. G. *Organometallics* **1998**, *17*, 3091.
(21) Wakatsuki, Y.; Koga, N.; Yamazaki, H.; Morokuma, K. *J. Am. Chem. Soc.* **1994**, *116*, 8105.
(22) (a) Farrugia, L. J. *J. Appl. Crystallogr.* **1999**, *32*, 837. (b) Farrugia, L. J. *J. Appl. Crystallogr.* **1997**, *30*, 565.
(23) Sheldrick, G. M. *Acta Crystallogr.* **2008**, *A64*, 112.
(24) (a) *Turbomole*, V6.5; Turbomole GmbH: Karlsruhe, Germany, 2013. (b) Ahlrichs, R.; Bar, M.; Haser, M.; Horn, H.; Kolmel, C. *Chem. Phys. Lett.* **1989**, *162*, 165.
(25) Becke, A. D. *Phys. Rev. A: At., Mol., Opt. Phys.* **1988**, *38*, 3098.
(26) Perdew, J. P. *Phys. Rev. B: Condens. Matter Mater. Phys.* **1986**, *33*, 8822.
(27) Eichkorn, K.; Weigend, F.; Treutler, O.; Ahlrichs, R. *Theor. Chem. Acc.* **1997**, *97*, 119.
(28) Schaefer, A.; Horn, H.; Ahlrichs, R. *J. Chem. Phys.* **1992**, *97*, 2571.
(29) Andrae, D.; Haeussermann, U.; Dolg, M.; Stoll, H.; Preuss, H. *Theor. Chim. Acta* **1990**, *77*, 123.
(30) Grimme, S.; Antony, J.; Ehrlich, S.; Krieg, H. *J. Chem. Phys.* **2010**, *132*, 154104.
(31) Grimme, S.; Ehrlich, S.; Goerigk, L. *J. Comput. Chem.* **2011**, *32*, 1456.
(32) Lee, C.; Yang, W.; Parr, R. G. *Phys. Rev. B* **1988**, *37*, 785.
(33) Klamt, A.; Schüürmann, G. *J. Chem. Soc., Perkin Trans.* **1993**, *2*, 799.